

Vortex phases in mesoscopic cylinders with suppressed surface superconductivity

W. V. Pogosov

*Moscow Institute of Physics and Technology,
141700 Dolgoprudnyi, Moscow region, Russia*

Vortex structures in mesoscopic cylinder placed in external magnetic field are studied under the general de Gennes boundary condition for the order parameter corresponding to the suppression of surface superconductivity. The Ginzburg-Landau equations are solved based on trial functions for the order parameter for vortex-free, single-vortex, multivortex, and giant vortex phases. The equilibrium vortex diagrams in the plane of external field and cylinder radius and magnetization curves are calculated at different values of de Gennes "extrapolation length" characterizing the boundary condition for the order parameter. The comparison of the obtained variational results with some available exact solutions shows good accuracy of our approach.

PACS numbers: 74.60.Ec, 74.24.Ha

I. INTRODUCTION

Recent achievements in electronic device miniaturization allow one to study the mesoscopic superconducting samples with sizes of the order of the coherence length $\xi(T)$. Such structures attract a considerable current interest as a possible basis for low temperature electronics. The superconducting state was studied experimentally for different-shaped samples: discs, loops, double loops, dots etc. [1–4]. It was shown that the sample shape and sizes affect significantly the phase diagrams of the mesoscopic superconductors.

The vortex phases in mesoscopic superconductors are commonly studied within the framework of the Ginzburg-Landau theory [5–17]. As it is well-known from the microscopic theory, the Ginzburg-Landau approach gives accurate results provided that the order parameter undergoes only slight spatial variation on the length scale of $\xi(0)$. This means that the Ginzburg-Landau theory can be used in the temperature range not far from T_c . However, it is known from the experience that it is also able to give reasonable results beyond this limit. The Ginzburg-Landau solutions for axially symmetric mesoscopic samples (cylinders, discs) can be subdivided into two different types [6–11]. In the first case the modulus of the local order parameter is axially symmetric inside the sample. The superconducting vortex-free state, the single-vortex state, and the giant-vortex state belong to this type of solutions. In the second case the axial symmetry is broken and a vortex cluster is formed inside the

sample (multivortex phase). This state usually appears at lower fields and larger sample sizes as compared to the giant-vortex phase [7,8,10,11]. Note that multivortex state corresponds to the Abrikosov flux-line lattice for the bulk superconductors.

The phase diagram of mesoscopic superconductor is strongly influenced by the boundary condition for the order parameter. In general case it is given by the de Gennes boundary condition [18,19]:

$$\mathbf{n}(-i\nabla - \mathbf{A})\psi = \frac{i}{b}\psi, \quad (1)$$

where \mathbf{n} is the unit vector normal to the sample surface, b is the de Gennes "extrapolation length", \mathbf{A} is the vector potential, and ψ is the order parameter. Here and below the following dimensionless variables are used: distances, magnetic field, and the order parameter are measured in units of coherence length $\xi(T)$, bulk upper critical field H_{c2} , and $\sqrt{-\alpha/\beta}$, respectively, with α , β being the Ginzburg-Landau coefficients. The "extrapolation length" b has a physical meaning of a length scale of the order parameter variation at the sample surface. Microscopic considerations show that b depends on the properties of interface, it is maximum for an ideal surface with the mirror reflection of quasi-particles and minimum for the rough surface with the diffusive reflection [18–21]. For the superconductor-dielectric (or vacuum) interface we have $b \rightarrow \infty$ in the former case and $b \sim \xi(0)$ in the latter case. The value of b depends also on the surface orientation provided that a superconducting gap is anisotropic. It follows from Eq. (1) that the order parameter is suppressed in the vicinity of the sample surface at $b \sim \xi(0)$. For the superconductor-normal metal interface b is always small, $b \sim \xi(0)$, because of diffusion of normal electrons from the metal to the superconductor. The "extrapolation length" b in this case is a function of temperature and various characteristics of metal and interface [19–23]. There are also possibilities for the enhancement of the order parameter at the interface that can be described by negative b values. It can be realized by choosing the suitable material as a surrounding medium [24,25], i.e., a superconductor having a higher transition temperature than the material of the mesoscopic sample. Another possibility is to use a semiconductor as a surrounding medium, such that there is an overlap of the band gap of the semiconductor with the superconducting gap. For the case of isotropic superconductor-vacuum ideal interface ($b \rightarrow \infty$), the magnetic properties of mesoscopic cylinders and discs, their equilib-

rium and non-equilibrium phase diagrams were studied in numerous papers, see e.g. Refs. [5–15], using different approaches. The vortex structures allowing for the *enhanced* surface superconductivity were studied in Refs. [24,25]. In Ref. [24] the case of mesoscopic discs was considered within the lowest Landau level approximation, which first was proposed in Refs. [7,10]. In Ref. [25] the Ginzburg-Landau equations were solved numerically and self-consistently for superconducting state in long cylinders.

In this paper we focus on magnetic properties of mesoscopic cylinders under the general boundary condition for the order parameter corresponding to the opposite case of *suppressed* surface superconductivity. For this purpose, we propose a variational approach and solve the Ginzburg-Landau equations without straightforward integration using trial functions for the order parameter. These trial functions involve a set of variational parameters yielding, as we show, more accurate quantitative description of the spatial distribution of the order parameter than frequently used lowest Landau level approximation. The approach is applicable to all vortex phases (the vortex-free, the single-vortex, the multivortex, and the giant vortex states) and any values of de Gennes "extrapolation length". The comparison of variational calculations with some available exact results demonstrates good accuracy of our approximation. The model enables us to calculate the equilibrium H_e - R diagram of the cylinder, where H_e is the external field and R is the cylinder radius. The magnetization curves of the cylinder are calculated.

II. MODEL

Let us consider a cylindrical type-II superconductor placed in the uniform external magnetic field H_e parallel to the cylinder axis. The sample is assumed to be much longer than London penetration depth $\lambda(T)$. Therefore, both the order parameter and the magnetic field are constant along cylinder axis. We use the cylindrical coordinate system with coordinates r , φ , z and unit vectors \mathbf{e}_r , \mathbf{e}_φ , \mathbf{e}_z .

The system of Ginzburg-Landau equations is given by [26]:

$$|\psi|^2 \psi - \psi + (i\nabla + \mathbf{A})^2 \psi = 0, \quad (2)$$

$$\text{rot } \mathbf{H} = \frac{1}{\kappa^2} \left[\mathbf{A}|\psi|^2 + \frac{i}{2} (\psi^* \nabla \psi - \psi \nabla \psi^*) \right], \quad (3)$$

where \mathbf{H} and ψ are the dimensionless local magnetic field and the order parameter ($\mathbf{H} = \text{rot } \mathbf{A}$, $\mathbf{H} = H_e \mathbf{e}_z$); $\kappa = \lambda(T)/\xi(T)$ is the Ginzburg-Landau parameter. Equations (2) and (3) must be supplemented by the boundary conditions for the order parameter (1) and the magnetic field:

$$H(R) = H_e. \quad (4)$$

Next, we expand all variables in powers of κ :

$$\psi = \sum_{n=0}^{\infty} \psi_{2n} \frac{1}{\kappa^{2n}}, \quad \mathbf{A} = \sum_{n=0}^{\infty} \mathbf{A}_{2n} \frac{1}{\kappa^{2n}}, \quad H = \sum_{n=0}^{\infty} H_{2n} \frac{1}{\kappa^{2n}}. \quad (5)$$

We substitute expansions (5) to Ginzburg-Landau equations (2), (3) and to boundary conditions (1), (4) and equate powers of κ . It is easy to show that the vector potential and the magnetic field at leading order are given by:

$$\mathbf{A}_0 = \mathbf{e}_\varphi \frac{H_e r}{2}, \quad H_0 = H_e. \quad (6)$$

The order parameter at leading order ψ_0 is determined by the first Ginzburg-Landau equation (2) and the boundary condition (1) at $\mathbf{H} = \mathbf{H}_0$. This condition is now given by:

$$\frac{\partial \psi_0}{\partial r} + \frac{\psi_0}{b} = 0. \quad (7)$$

In the next order one has from Eq. (3):

$$H_2 = - \int_0^r dr \mathbf{e}_\varphi \left[|\psi_0|^2 \mathbf{A}_0 + \frac{i}{2} (\psi_0^* \nabla \psi_0 - \psi_0 \nabla \psi_0^*) \right]. \quad (8)$$

Thus, at leading order the magnetic field is uniform inside the sample and the magnetization equals zero. Physically, this implies that the additional field generated by the Meissner current and by the vortices is of the order of $1/\kappa^2$ in comparison with the external uniform field. Below, we shall calculate the energy of the sample at leading order, whereas the magnetization will be found at the next order using Eq. (8). It was shown in Ref. [27] that this approximation is accurate not only for high- κ materials but also for moderate- κ superconductors (e.g. $\kappa \approx 4$) with sizes comparable to $\xi(T)$.

We present ψ_0 as a Fourier series:

$$\psi_0(r, \varphi) = \sum_{L_j=0}^{\infty} f_{L_j}(r) \exp(-iL_j \varphi). \quad (9)$$

For the axial symmetric distribution of the modulus of the order parameter inside the sample the only one term in Eq. (9) is nonzero. The vortex-free, single-vortex, and giant vortex phases with angular quantum momentum L correspond to the harmonics with $L_j = 0, 1$, and L , respectively. The modulus of the order parameter in the multivortex phase is not axially symmetric. Note that in this case the symmetry of the vortex configuration imposes a restriction on functions f_{L_j} : some of these functions equal zero. It was shown in Refs. [7,10] that taking into account only two main terms in right-hand side of Eq. (9) is enough for an accurate calculation of

the energy of the mesoscopic superconductor in multivortex state. The vortex cluster with L vortices on a ring and no vortex at the axis (ring-like configuration) can be described as a mixture of two components with $L_1 = 0$ and $L_2 = L$ ($(0 : L)$ state). The vortex cluster with one vortex at the cylinder axis and $(L - 1)$ vortices on a ring corresponds to $L_1 = 1$ and $L_2 = L$ ($(1 : L)$ state). The contribution from other harmonics is small and can be neglected, when we consider few-fluxoid cylinders that can accommodate just few vortices [7,10].

Using Eqs. (2) and (9) it can be easily shown that each function $f_{L_j}(r)$ has the following asymptotic at $r \rightarrow 0$:

$$f_{L_j}(r) \sim r^{L_j}. \quad (10)$$

Besides, each function $f_{L_j}(r)$ meets boundary condition (7). These conditions for $f_{L_j}(r)$ are valid both for the giant vortex and the multivortex phases. It is a rather complicated task to find $f_{L_j}(r)$ from the first Ginzburg-Landau equation (2) due to its non-linearity. Instead of the straightforward integration of this equation, it is possible to use trial functions for the coordinate dependence $f_{L_j}(r)$. Notice that different variational procedures allowing one to solve approximately the Ginzburg-Landau equations were used in numerous papers for mesoscopic [7,10,15], bulk [28–31], and different-shaped [32] superconductors. One can easily show that if Eq. (9) is a solution of the first Ginzburg-Landau equation, each function $f_{L_j}(r)$ can be represented as the following series expansion in powers of r/R without loss of generality:

$$f_{L_j}(r) = \exp\left(-q_{L_j} \frac{r^2}{R^2}\right) \sum_{u=0}^{\infty} p_u^{L_j} \left(\frac{r}{R}\right)^{L_j+2u}, \quad (11)$$

where $p_u^{L_j}$ are constants. The value of q_{L_j} can be found from boundary condition (7):

$$q_{L_j} = \frac{R}{2b} + \frac{1}{2} \frac{\sum_{u=0}^{\infty} p_u^{L_j} (L_j + 2u)}{\sum_{u=0}^{\infty} p_u^{L_j}}. \quad (12)$$

Our approach is to consider the coefficients $p_u^{L_j}$ as variational parameters and to minimize the free energy with respect to $p_u^{L_j}$. The exponential prefactor in Eq. (11) takes into account the suppression of the order parameter at the contact with a surrounding material. First term in the expansion describes the behavior of the order parameter in the central part of the sample. Other terms specify the order parameter in the sample as a whole. As it will be shown below, taking into account only first three terms in Eq. (11) is enough for the accurate calculation of the order parameter distribution, and we will use this approximation in all calculations of magnetization and H_e - R diagrams. Note that trial function (11) was used in Ref. [32] for the study of surface superconductivity in samples of different complex shapes placed in vacuum ($b \rightarrow \infty$).

The Ginzburg-Landau functional for the Gibbs free energy G of the cylinder can be written as a sum of two

contributions, G_b and G_s . The former is the bulk energy of the sample and the latter is the surface energy. These contributions are given by [20,23,26]:

$$G_b = \int \left[-|\psi|^2 + \frac{1}{2}|\psi|^4 + |(-i\nabla - \mathbf{A})\psi|^2 + \kappa^2 \mathbf{H}^2 - 2\kappa^2 \mathbf{H} \mathbf{H}_e \right] dV, \quad (13)$$

$$G_s = \frac{1}{b} \int |\psi|^2 dS. \quad (14)$$

The integration in Eqs. (13) and (14) is performed over the sample bulk and surface, respectively. Note that the general boundary condition for the order parameter (1) can be obtained phenomenologically by minimization of the free energy functional $G = G_b + G_s$ with respect to the order parameter ψ and the vector potential \mathbf{A} [20,23,33].

Substituting expansion (9) to Eqs. (13) and (14) and taking into account Eq. (6) we obtain the expression for the energy of the multivortex state (per unit length of the cylinder):

$$G_b = 2\pi \int_0^R r dr \left[\frac{1}{2} (f_{L_1}^4 + f_{L_2}^4 + 4f_{L_1}^2 f_{L_2}^2) - f_{L_1}^2 - f_{L_2}^2 + \left(\frac{df_{L_1}}{dr}\right)^2 + \left(\frac{df_{L_2}}{dr}\right)^2 - \kappa^2 H_e^2 + f_{L_1}^2 \left(\frac{H_e r}{2} - \frac{L_1}{r}\right)^2 + f_{L_2}^2 \left(\frac{H_e r}{2} - \frac{L_2}{r}\right)^2 \right], \quad (15)$$

$$G_s = \frac{2\pi R}{b} (f_{L_1}^2(R) + f_{L_2}^2(R)). \quad (16)$$

The energy of any state having axially symmetric modulus of the order parameter with angular momentum L reduces to Eqs. (15) and (16). In this case we must put $L_1 = L$, $f_{L_2} = 0$. Using Eqs. (11) and (12) we find the energy G from Eqs. (15) and (16) by a straightforward integration as an explicit function of variational parameters $p_0^{L_1}$, $p_1^{L_1}$, $p_2^{L_1}$ and $p_0^{L_2}$, $p_1^{L_2}$, $p_2^{L_2}$. The resulting expression, however, is rather cumbersome and we do not present it here. Finally, values of the variational parameters at each R are found numerically by the minimization of the free energy. This procedure yields the local order parameter and the energy of the cylinder.

Knowing the local order parameter we can calculate the magnetization. It is given by:

$$-4\pi M = \langle H \rangle - H_e, \quad (17)$$

where $\langle H \rangle$ is the averaged magnetic field over the superconductor volume. Taking into account Eq. (8) and expansion (9) we obtain:

$$-4\pi M = \frac{2}{\kappa^2 R^2} \int_0^R r dr \int_0^r dx \left[f_{L_1}^2(x) \left(\frac{H_e x}{2} - \frac{L_1}{x} \right) + f_{L_2}^2(x) \left(\frac{H_e x}{2} - \frac{L_2}{x} \right) \right]. \quad (18)$$

Functions f_{L_1} and f_{L_2} are found by the method described above. Hence, one can calculate the magnetization using Eq. (18). In the following section we apply the developed approach for the analysis of the behavior of the cylinder in the external field.

III. RESULTS AND DISCUSSION

Comparing the energies of different states one can calculate the equilibrium H_e - R diagram of the cylinder. The results of our calculations are shown in Fig. 1 for different b values: $b = 1$ (a), $b = 2.5$ (b), $b = 5$ (c), and $b \rightarrow \infty$ (d). The latter case corresponds to the isotropic superconductor-vacuum ideal interface, and was studied in Refs. [5,6,10,11,13–15]. Curve 1 shows the transition from the normal to the superconducting state (the surface critical field H_{c3}). The oscillatory behavior of the function $H_{c3}(R)$ is caused by the fact that the transition occurs from the normal to the giant vortex states with different angular quantum moments L depending on the cylinder radius. Besides, the function $H_{c3}(R)$ depends appreciably on the value of b : the value of $H_{c3}(R)$ decreases with decrease of b . At $R \rightarrow \infty$ the dependence $H_{c3}(R)$ tends to the surface critical field for the half-space sample, which was calculated in Ref. [22] as a function of b . Note that $H_{c3}(\infty) = 1.695$ for $b \rightarrow \infty$ and $H_{c3}(\infty) = 1$ for $b \rightarrow 0$ [18,22].

Below H_{c3} the transitions between different giant vortex states take place. Solid lines show the phase boundaries between the states with different vorticities that are the sums of angular quantum moments of all vortices and giant vortices. In the giant vortex state the order parameter is strongly suppressed in the inner part of the cylinder, and this state can be referred to a surface superconductivity. For illustration, the spatial distribution of the order parameter in the giant vortex phase with $L = 2$ is plotted in Fig. 2 at $b = 1$, $R = 3.9$, $H_e = 0.9$ (a) and $b \rightarrow \infty$, $R = 4.56$, $H_e = 0.5$ (b) (solid lines). In the former case the order parameter is also suppressed at the sample surface because of the small b value (e.g., superconductor-normal metal interface). To check the accuracy of our approach we took into account next several terms in expansion (11), thus increasing the number of variational parameters. As we found, this practically did not change the calculated order parameter for almost all points of H_e - R diagram shown in Fig. 1. This result implies that our variational calculations are close to the exact solutions of the Ginzburg-Landau equations since expansion (11) is written without any loss of generality. Therefore, one can find Ginzburg-Landau solution with

any desired accuracy (for the states with axially symmetric modulus of the order parameter) allowing for enough number of variational parameters $p_u^{L_j}$. For multivortex states the accuracy is limited by the fact that we take into account only two main harmonics in the Fourier expansion (9). In Fig. 2 we also plotted the spatial variation of the order parameter calculated within the lowest Landau level approximation (dashed lines). In this approximation the order parameter is proportional to the eigenfunction of the kinetic energy operator corresponding to the lowest eigenvalue. We found that this approach remains very accurate not far from H_{c2} and H_{c3} (see Fig. 2(a)). At lower fields the results of the lowest Landau level approximation are not so accurate (Fig. 2(b)).

As follows from Fig. 1, the superconducting state does not nucleate at very small cylinder radii, smaller than some critical radius, and the sample is in normal state at any applied field. The critical radius tends to zero at $b \rightarrow \infty$. There is also the interval of R for each b , when the vortex phase does not nucleate, and the transition occurs from the normal to the superconducting vortex-free state. Every vortex phase with vorticity $L > 1$ can exist in the form of the giant vortex or the multivortex configuration. The dashed lines on Fig. 1 show the boundaries between these states. Below these lines for given $L > 1$ the multivortex state has the lowest energy, and above these curves the giant vortex state becomes more energetically favorable. In equilibrium state the multivortex phase can exist if the applied field is smaller than 1 (H_{c2} in dimensional units) and if the radius of the cylinder is large enough. For each b there exists an interval of small cylinder radii, when the multivortex phase is energetically unfavorable as compared to the states with axial symmetric distribution of the modulus of the order parameter. Curve 2 in Fig. 1 shows the lower critical field that corresponds to the equilibrium boundary between the vortex-free and the single-vortex states.

With increasing the external field the cylinder can follow rather complex set of phase transitions. It can come from the giant vortex to the multivortex states and then back to the giant vortex phase. For example, at $R = 4.4$, $b = 1$ the following set of transitions occurs: $0 \rightarrow 1 \rightarrow (0:2) \rightarrow 2 \rightarrow (0:3) \rightarrow 3 \rightarrow (0:4) \rightarrow 4$. At $R = 4.1$, $b = \infty$ the set of transitions is: $0 \rightarrow 1 \rightarrow 2 \rightarrow (0:3) \rightarrow 3 \rightarrow (0:4) \rightarrow 4 \rightarrow 5 \rightarrow 6 \rightarrow 7 \rightarrow 8 \rightarrow 9 \rightarrow 10 \rightarrow 11$.

The transitions between the phases with different vorticities are always discontinuous, they occur when the energies of different states become equal. The transitions between the states with the same vorticity may be continuous as well as discontinuous. Continuous phase transitions occur between the multivortex and the giant vortex states. In this case, with increasing of the applied field the intervortex distances decrease, and vortices merge into the giant vortex located at the cylinder axis. The similar results were obtained in Refs. [7–11] for the case $b = \infty$ and in Ref. [24] at $b < 0$ (enhanced surface superconductivity). In our calculations we also

took into account a possibility of existence of the multivortex clusters with central vortex. It turned out that such configurations can be more favorable energetically than giant vortex states in some regions of H_e - R diagram shown in Fig. 1. However, in all these cases the ring-like clusters have the lower energy. For cylinders thicker than shown in Fig. 1 we found that at any $b > 0$ the ground state can be represented by configurations with the central vortex. The transitions between multivortex states of the same vorticity with and without central vortex are discontinuous.

With increasing of the cylinder radius the number of vortices, which it is able to accommodate, increases, and finally vortex array transforms to the classical triangular Abrikosov flux-line lattice far from the surface. The first step on this way is the appearance of the clusters with central vortex. However, we do not analyze here the transition from the mesoscopic to the macroscopic behavior and restrict ourselves on few-fluxoid cylinders, which can accommodate only few vortices before the transition to the normal state and whose magnetic properties can be described in terms of mixture of only two harmonics in Eq. (9).

Now we find the magnetization of the cylinder using Eq. (18). The results of our calculations at $\kappa = 5$ are presented in Fig. 3(a) for $b = 1$, $R = 4.625$ and in Fig. 4(a) for $b \rightarrow \infty$, $R = 4.05$. In these cases the cylinders accommodate the giant vortices with maximum angular quantum moments equal to 5 and 11, respectively, before the transition to the normal state. Jumps in the magnetization correspond to the transitions between the states with different vorticity. It is interesting that in the state with suppressed surface superconductivity (Fig. 3(a)) the discontinuity of the field dependence of the magnetization is less pronounced, especially at high fields. In the first case (Fig. 4(a)) at $H_e \approx 0.61$ ($0.61H_{c2}$ in dimensional units) the transition occurs from the multivortex state with 2 vortices to the giant vortex state with angular quantum momentum 2 ($2 \rightarrow (0:2)$). In the second case (Fig. 4(b)) the transition $3 \rightarrow (0:3)$ occurs at $H_e \approx 0.74$ and the transition $4 \rightarrow (0:4)$ occurs at $H_e \approx 0.87$. All these transitions are followed by weak jumps in the slope of the magnetization. The behavior of the magnetization near the transitions is shown in Fig. 3(b) and 4(b). Solid lines denote the equilibrium magnetization, dashed lines denote the metastable magnetization corresponding to the giant vortex phase. The similar behavior of the magnetization in the vicinity of the multivortex-giant vortex transitions was reported in Ref. [34] for the case $b \rightarrow \infty$.

Next we discuss the accuracy of our variational procedure. First, we compare the variational results with known exact solutions for the surface critical field. The phases with axial symmetric distribution of the modulus of the order parameter are always energetically more favorable with respect to the multivortex state at applied field higher than the bulk upper critical field (see phase diagrams on Fig. 1). In the vicinity of the surface critical field the first Ginzburg-Landau equation (1) can be lin-

earized. A resulting equation has the following analytical solution [5]:

$$f_L(R) = r^L \exp\left(-\frac{H_e r^2}{4}\right) \Phi\left(\frac{H_e - 1}{2H_e}, L + 1, \frac{H_e r^2}{2}\right), \quad (19)$$

where Φ is Kummer function. Function (19) must meet the boundary condition (7). This yields the transcendental equation for the surface critical field allowing one to find $H_{c3}(R)$ exactly. The comparison of the variationally calculated H_{c3} with this exact dependence shows good agreement with an accuracy better than 1% for all values of b and R under study. The lower critical field of the cylinder H_{c1} versus R was calculated numerically in Ref. [12] at $b \rightarrow \infty$. The comparison of this result with our dependence $H_{c1}(R)$ reveals the same accuracy. Thus, our results appear to be a good approximation to the exact Ginzburg-Landau solutions for the mesoscopic cylinders.

In summary, we analyzed the superconducting state in long mesoscopic cylinder with suppressed surface superconductivity. An asymptotic expansion was used to simplify the Ginzburg-Landau equations at high and moderate values of κ , and the simplified equations were solved by variational method. The equilibrium H_e - R diagram of the cylinder were obtained, where H_e is the external field and R is the cylinder radius, at different values of "extrapolation length". We showed that magnetic properties of the cylinder depend appreciably on the value of "extrapolation length" and studied the evolution of H_e - R diagram with changing of "extrapolation length".

ACKNOWLEDGMENTS

The author acknowledges useful discussions with K. I. Kugel, A. L. Rakhmanov, and E. A. Shapoval. This work was supported by the Russian Foundation for Basic Research (RFBR), grants Nos. 00-02-18032 and 01-02-06526, by the joint INTAS-RFBR program, grant No. IR-97-1394, and by the Russian State Program 'Fundamental Problems in Condensed Matter Physics'.

-
- [1] V. V. Moshchalkov, L. Gielen, C. Strunk, R. Jonckheere, X. Qiu, C. Van Haesendonck, and Y. Bruynseraede, *Nature* **373**, 319 (1995).
 - [2] A. K. Geim, I. V. Grigorieva, S. V. Dubonos, J. G. S. Lok, J. C. Maan, A. E. Filippov, and F. M. Peeters, *Nature* **390**, 259 (1997).
 - [3] A. K. Geim, S. V. Dubonos, I. V. Grigorieva, K. S. Novoselov, F. M. Peeters, and V. A. Schweigert, *Nature* **407**, 55 (2000).

- [4] V. Bruyndoncx, C. Strunk, and V. V. Moshchalkov, *Europhys. Lett.* **36**, 449 (1996).
- [5] V. V. Moshchalkov, X. G. Qiu, and V. Bruyndoncx, *Phys. Rev. B* **55**, 11793 (1997).
- [6] V. A. Schweigert and F. M. Peeters, *Phys. Rev. B* **57**, 13817 (1998).
- [7] V. A. Schweigert, F. M. Peeters, and P. S. Deo, *Phys. Rev. Lett.* **81**, 2783 (1998).
- [8] V. A. Schweigert and F. M. Peeters, *Phys. Rev. Lett.* **83**, 2409 (1999).
- [9] A. K. Geim, S. V. Dubonos, and J. J. Palacios, *Phys. Rev. Lett.* **85**, 1528 (2000).
- [10] J. J. Palacios, *Phys. Rev. B* **52**, R5948 (1998).
- [11] J. J. Palacios, *Phys. Rev. Lett.* **84**, 1796 (2000).
- [12] E. A. Shapoval, *Pis'ma Zh. Eksp. Teor. Fiz.* **69**, 532 (1999) [*JETP Lett.* **69**, 577 (1999)].
- [13] G. F. Zharkov, V. G. Zharkov, and A. Yu. Zvetkov, *Phys. Rev. B* **61**, 12293 (2000).
- [14] G. F. Zharkov, *Phys. Rev. B* **63**, 224513 (2001).
- [15] W. V. Pogosov, A. L. Rakhmanov, and E. A. Shapoval, *Physica C* **356**, 225 (2001).
- [16] V. R. Misko, V. M. Fomin, J. T. Devreese, and V. V. Moshchalkov, *Solid State Commun.* **114**, 499 (2000).
- [17] V. M. Fomin, J. T. Devreese, V. Bruyndoncx, and V. V. Moshchalkov, *Phys. Rev. B* **62**, 9186 (2000).
- [18] P. G. de Gennes, *Superconductivity of Metals and Alloys* (Addison-Wesley, New York, 1994).
- [19] P. G. de Gennes and J. Matricon, *Rev. Mod. Phys.* **36**, 45 (1964).
- [20] E. A. Andrushin, V. L. Ginzburg, and A. P. Silin, *Usp. Fiz. Nauk* **163**, 105 (1997) [*Phys. Usp.* **36**, 854 (1993)].
- [21] R. O. Zaitsev, *Zh. Eksp. Teor. Fiz.* **48**, 1759 (1965) [*Sov. Phys. JETP* **21**, 1178 (1965)].
- [22] E. A. Shapoval, *Pis'ma Zh. Eksp. Teor. Fiz.* **64**, 320 (1996) [*JETP Letters* **64**, 350 (1996)].
- [23] V. P. Mineev and K. V. Samokhin, *The Introduction to the Theory of Unconventional Superconductors*, Moscow, 1996 [in Russian].
- [24] S. V. Yampolskii and F. M. Peeters, *Phys. Rev. B* **62**, 9663 (2000).
- [25] B. J. Baelus, S. V. Yampolskii, F. M. Peeters, E. Montevocchi, and J. O. Indekeu, *cond-mat/0106403* (2001).
- [26] D. Saint-James and G. Sarma, *Type II superconductivity*, Pergamon Press, 1969.
- [27] S. J. Chapman, Q. Du, M. D. Gunzburger, and J. S. Peterson, *Adv. Math. Sciences Appl.* **5**, 193 (1995).
- [28] H. Koppe and J. Willebrand, *J. Low Temp. Phys.* **2**, 499 (1970).
- [29] J. R. Clem, *J. Low Temp. Phys.* **18**, 427 (1975).
- [30] W. V. Pogosov, A. L. Rakhmanov, and K. I. Kugel, *Zh. Eksp. Teor. Fiz.* **118**, 676 (2000) [*JETP* **90**, 588 (2000)].
- [31] W. V. Pogosov, K. I. Kugel, A. L. Rakhmanov, and E. H. Brandt, *Phys. Rev. B* **64**, 064517 (2001).
- [32] R. C. Jones, M. K. Keene, and P. Nurwanto, *Physica C* **298**, 140 (1998).
- [33] K. I. Kugel, W. V. Pogosov, and A. L. Rakhmanov, *Physica C* **339**, 10 (2000).
- [34] F. M. Peeters and V. A. Schweigert, *Physica C* **332**, 266 (2000).

FIGURE CAPTIONS

Fig.1. Equilibrium H_e - R diagram of the cylinder in the external magnetic field at $b = 1$ (a), $b = 2.5$ (b), $b = 5$ (c), $b \rightarrow \infty$ (d). Solid lines show the boundaries between the states with different vorticity. Dashed lines correspond to the boundaries between the multivortex and the giant vortex phases. Curves 1 and 2 show the surface and the first critical fields, respectively. The dot line denotes the bulk upper critical field.

Fig 2. The spatial distribution of the dimensionless modulus of the order parameter inside the mesoscopic cylinder in giant vortex state with angular quantum momentum $L = 2$ at $b = 1$, $R = 3.9$, $H_e = 0.9$ (a) and $b \rightarrow \infty$, $R = 4.56$, $H_e = 0.5$ (b) Solid lines correspond to our variational result, dashed lines to the results of the lowest Landau level approximation. The distance from the cylinder axis r is measured in units of the coherence length $\xi(T)$.

Fig. 3. The equilibrium magnetization of the cylinder with radius $R = 4.625$ versus applied field at $b = 1$, $\kappa = 5$. Jumps in the magnetization in Fig. 3(a) correspond to the transitions between the states with different vorticity. Fig. 3(b) shows the behavior of the magnetization in the vicinity of the continuous phase transition at $H_e \approx 0.61H_{c2}$ from the multivortex state with 2 vortices to the giant vortex phase with vorticity $L = 2$. Solid lines correspond to the equilibrium magnetization, dashed line shows the magnetization of the metastable giant vortex phase.

Fig. 4. The equilibrium field dependence of the magnetization of the cylinder with radius 4.05 at $b \rightarrow \infty$, $\kappa = 5$. In Fig. 4(b) the magnetization is plotted versus applied field near the transitions from the multivortex states to the giant vortex phases. Solid lines correspond to the equilibrium magnetization, dashed line shows the magnetization of the metastable giant vortex phase.

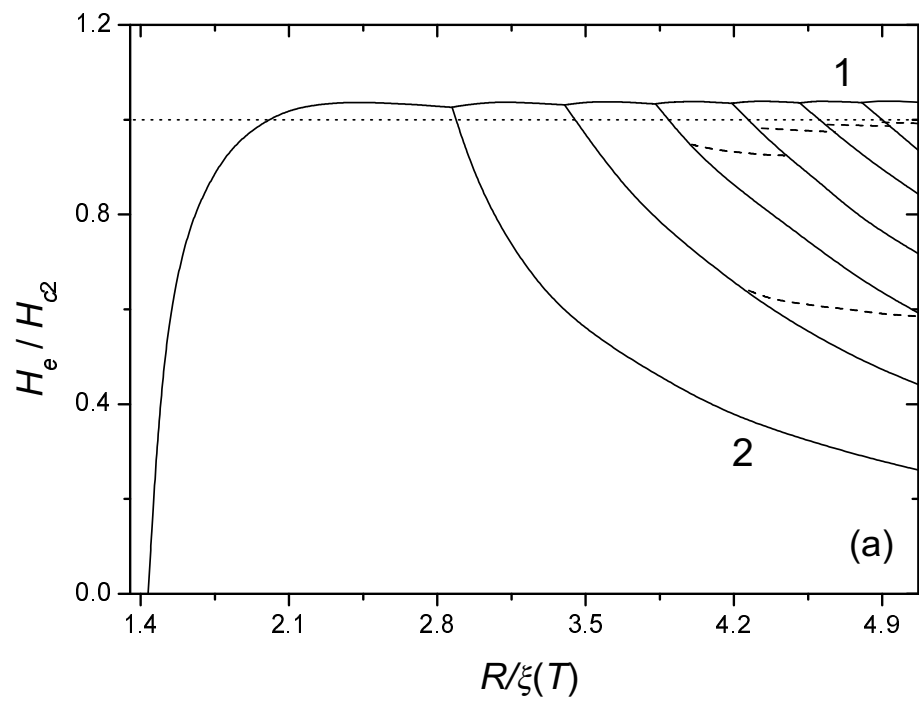


Fig. 1(a)

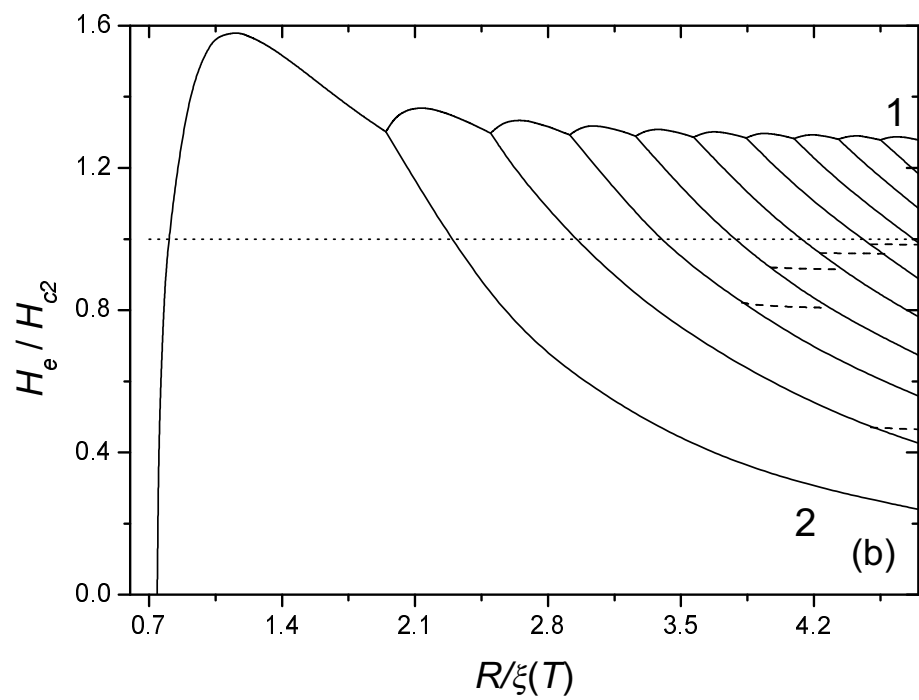


Fig. 1(b)

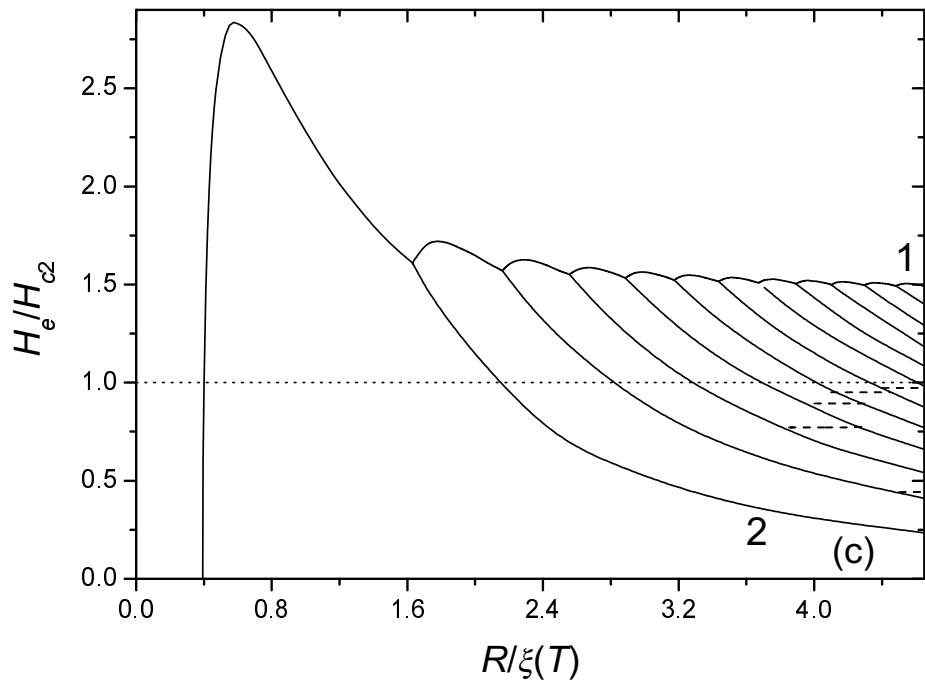


Fig. 1(c)

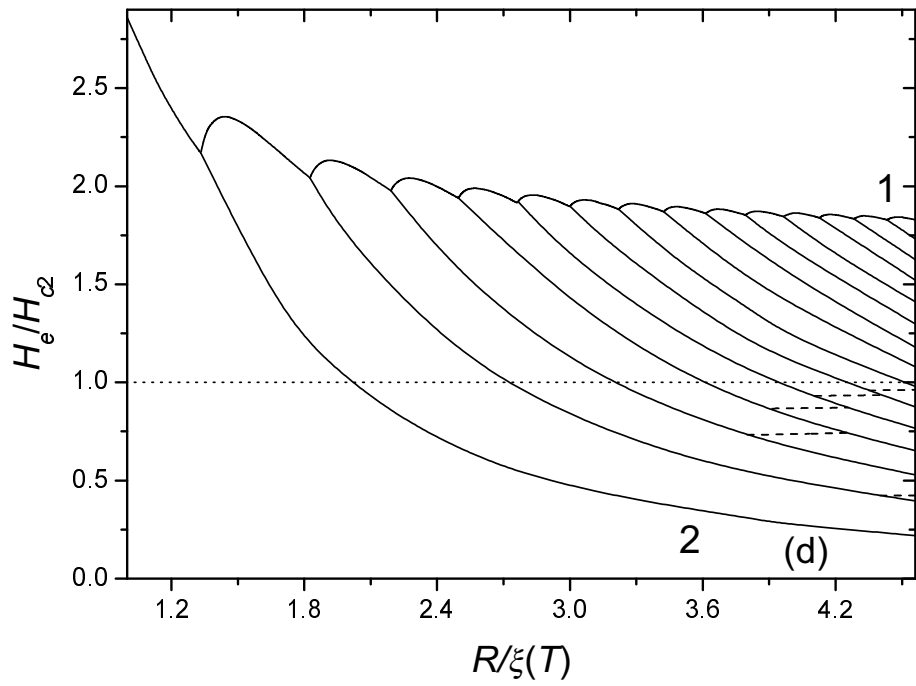


Fig. 1(d)

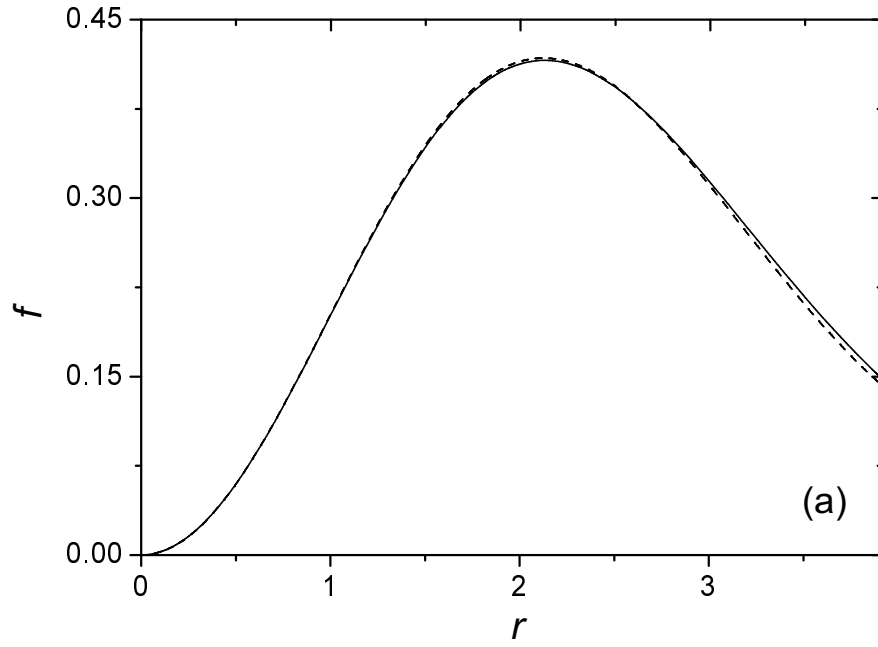


Fig. 2(a)

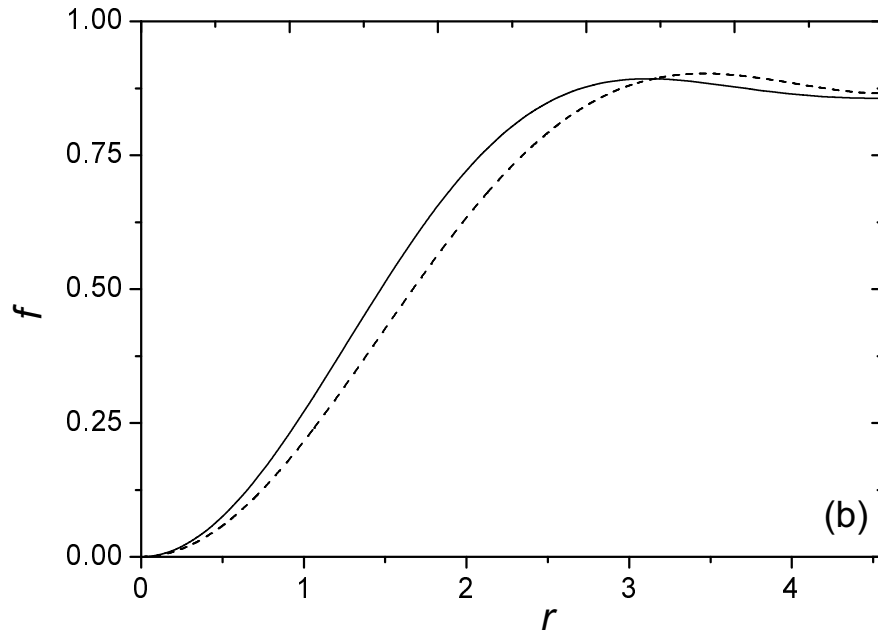


Fig. 2(b)

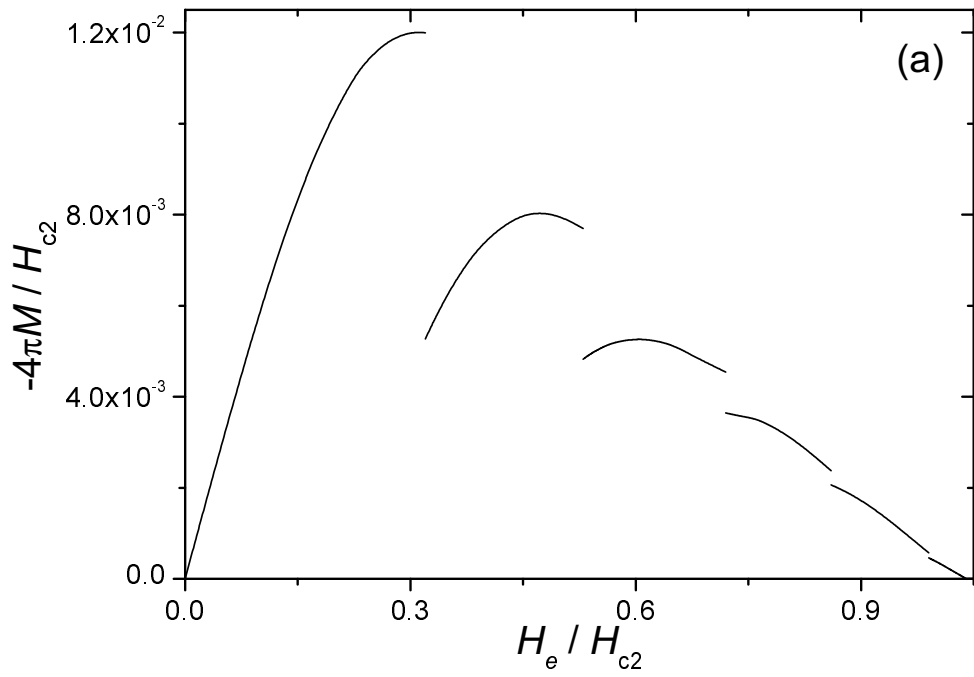


Fig. 3(a)

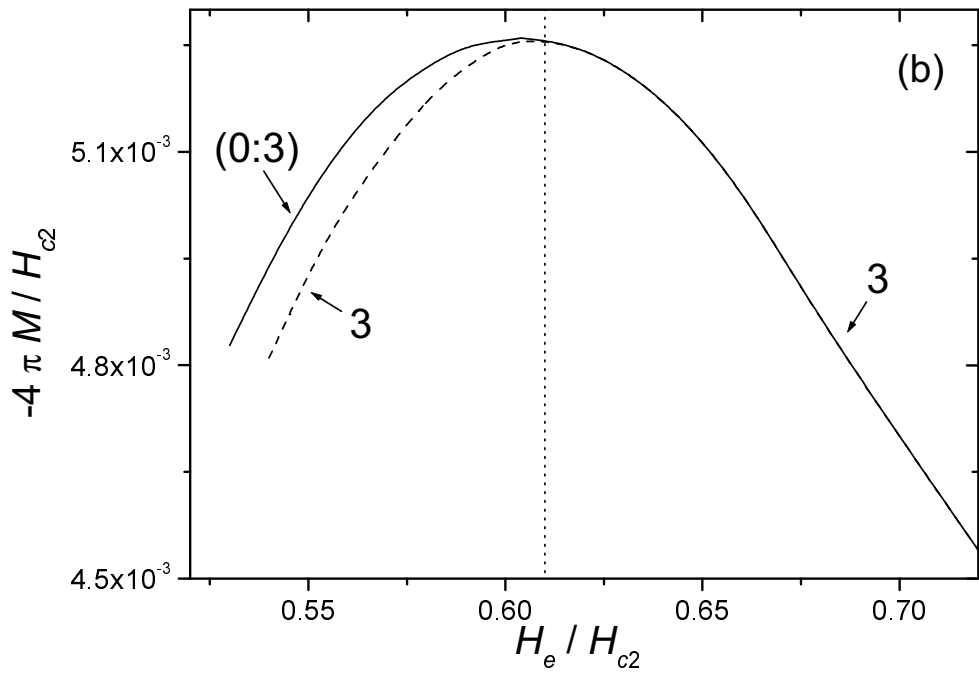


Fig. 3(b)

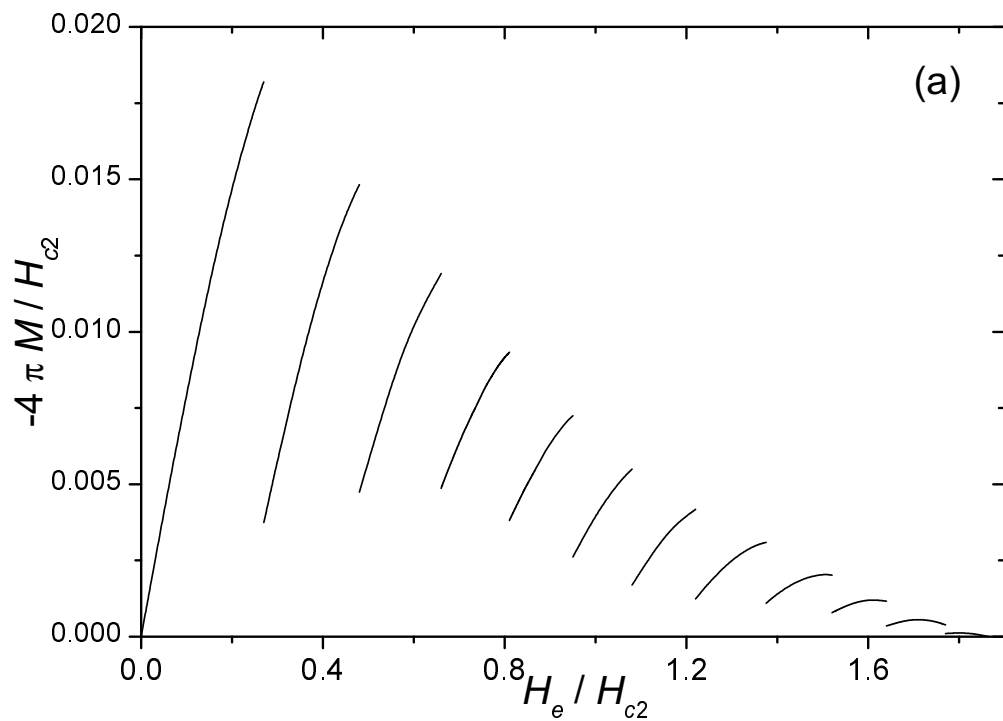


Fig. 4(a)

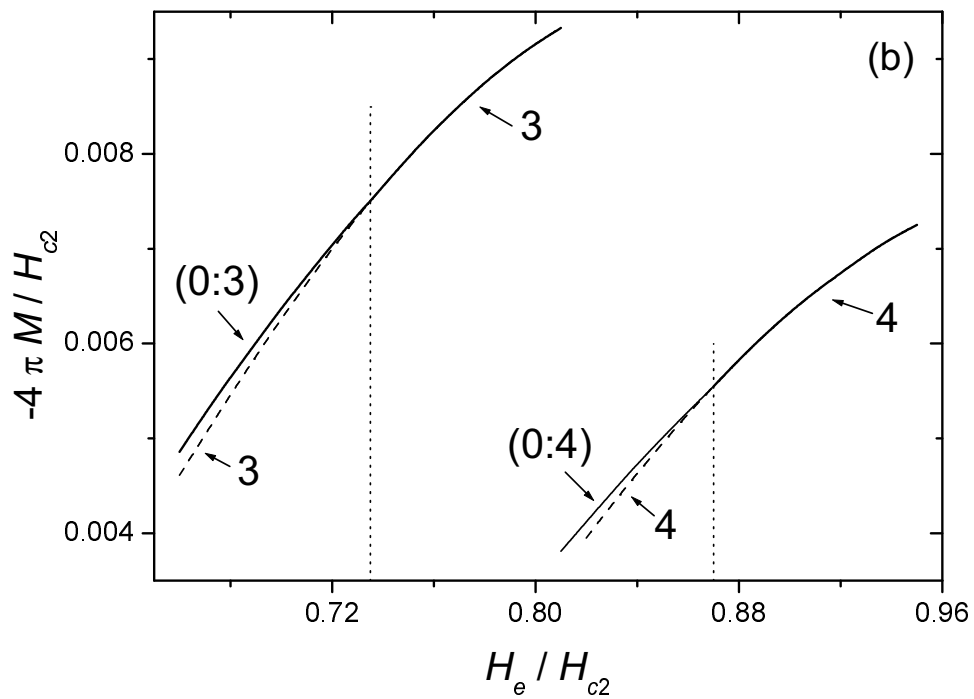


Fig. 4(b)